Supplementary information

Statistical organelle dissection of *Arabidopsis* guard cells using image database LIPS

Takumi Higaki*, Natsumaro Kutsuna, Yoichiroh Hosokawa, Kae Akita, Kazuo Ebine, Takashi Ueda, Noriaki Kondo, Seiichiro Hasezawa

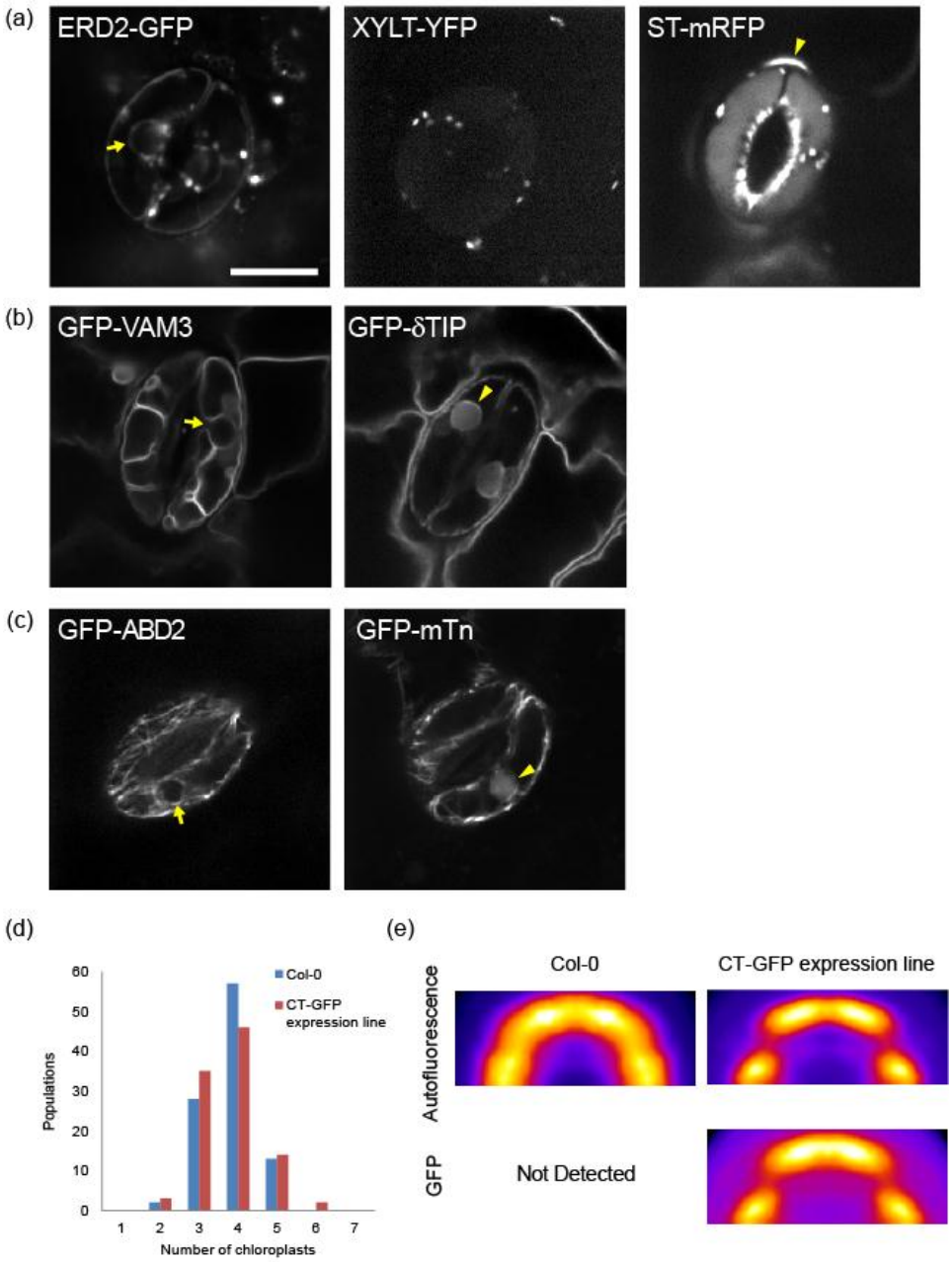

Supplementary Figure 1. Characterization of the fluorescent proteins and transgenic lines used in this study. (a) Comparison of the Golgi body markers. ERD2-GFP labeled the *cis*-Golgi and endoplasmic reticulum (ER) (arrow) as previously reported[41], whereas XYLT-YFP labeled the *medial*-Golgi. ST-mRFP labeled the *trans*-Golgi, vacuoles and apoplast (arrowhead) as previously reported[40]. (b) Comparison of

vacuolar membrane markers. GFP-δTIP labeled both the vacuolar membrane and ER (arrowhead) as reported previously[42]. The GFP-VAM3 did not label the ER as judged by a blank of perinuclear region (arrow). (c) Comparison of actin microfilament markers. GFP-mTn labeled both actin microfilaments and cell nuclei (arrowhead). GFP-ABD2 did not label the cell nuclei as judged by a blank of the spherical region (arrow). (d) Numbers of chloroplasts in a guard cell of wild type Col-0 and a CT-GFP expression line. Note that the numbers were slightly decreased by CT-GFP expression. Mean chloroplasts numbers were 3.81 and 3.77 in Col-0 and the GFP-CT expression line, respectively. (e) Probability maps of chloroplast autofluorescence and CT-GFP in Col-0 and CT-GFP expression line. Note that autofluorecence and CT-GFP showed similar patterns in CT-GFP line. These maps were obtained from group-averaged images from 100 guard cells, and are shown in pseudocolor.

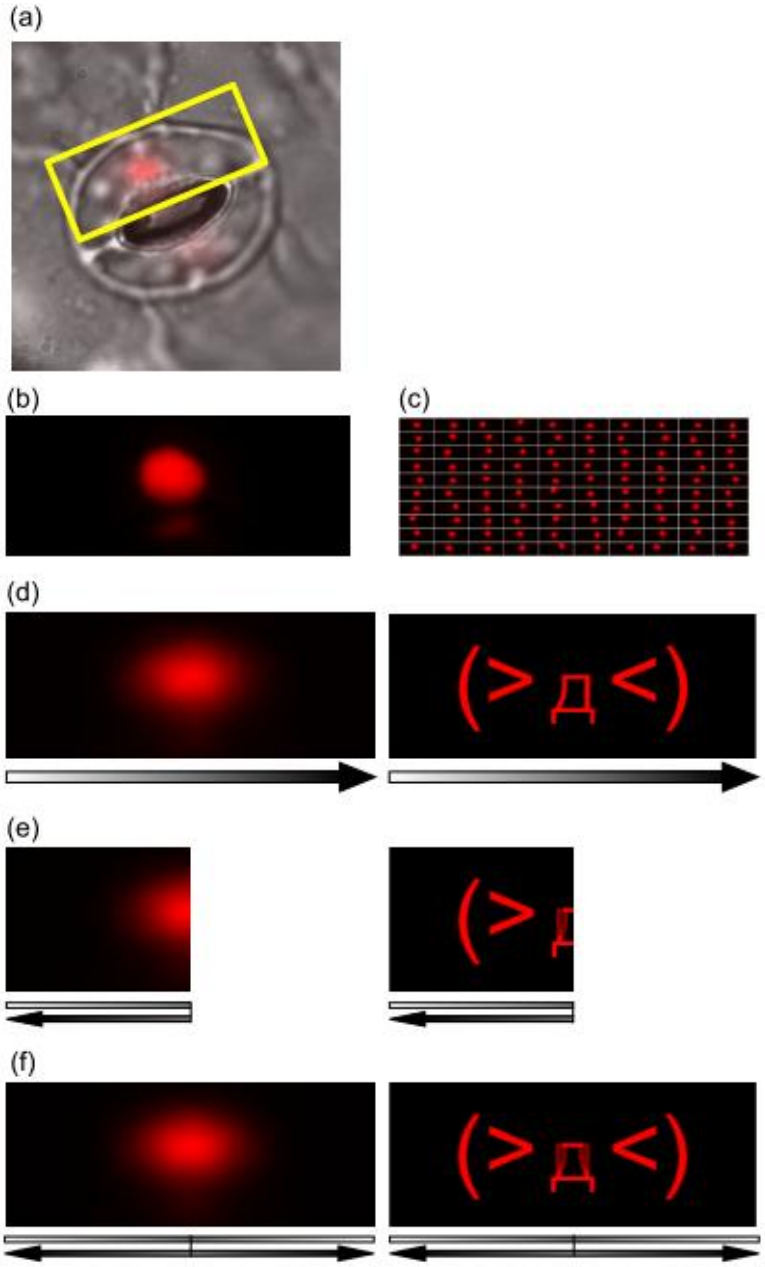

Supplementary Figure 2. Image processing for probability mapping with group-averaged images of guard cells. (a) Segmentation and normalization of a guard cell expressing HistoneH2B-RFP with a bounding box. We manually segmented each guard cell with a bounding box as shown in yellow. (b) Fluorescent image in the bounding box in (a). (c) Size- and intensity-normalized images. All the segmented images were interpolated to an average size of 19.5 × 7.6 μm (304 × 119 pixels), and

their fluorescent intensities normalized to an average intensity of 0 with a standard derivation of 1. (d) The group-averaged image of a cell nuclei labeled by HistoneH2B-RFP (left) and a Japanese face mark (right) as an example demonstrating subsequent image processing. Arrows delineate the major axis of the image. (e) Averaged images of the half-divided group-averaged images of cell nuclei (left) and the Japanese face mark (right). The inverted arrows show the directions of the half-separated images. (f) Probability map of the cell nuclei (left) and the Japanese face mark (right). The map was obtained as a symmetrical alignment of the averaged image of the half-separated images shown in (e). Note that the probability map is similar to the group-averaged images shown in (d) when the averaged images are symmetrical with respect to the major axis.

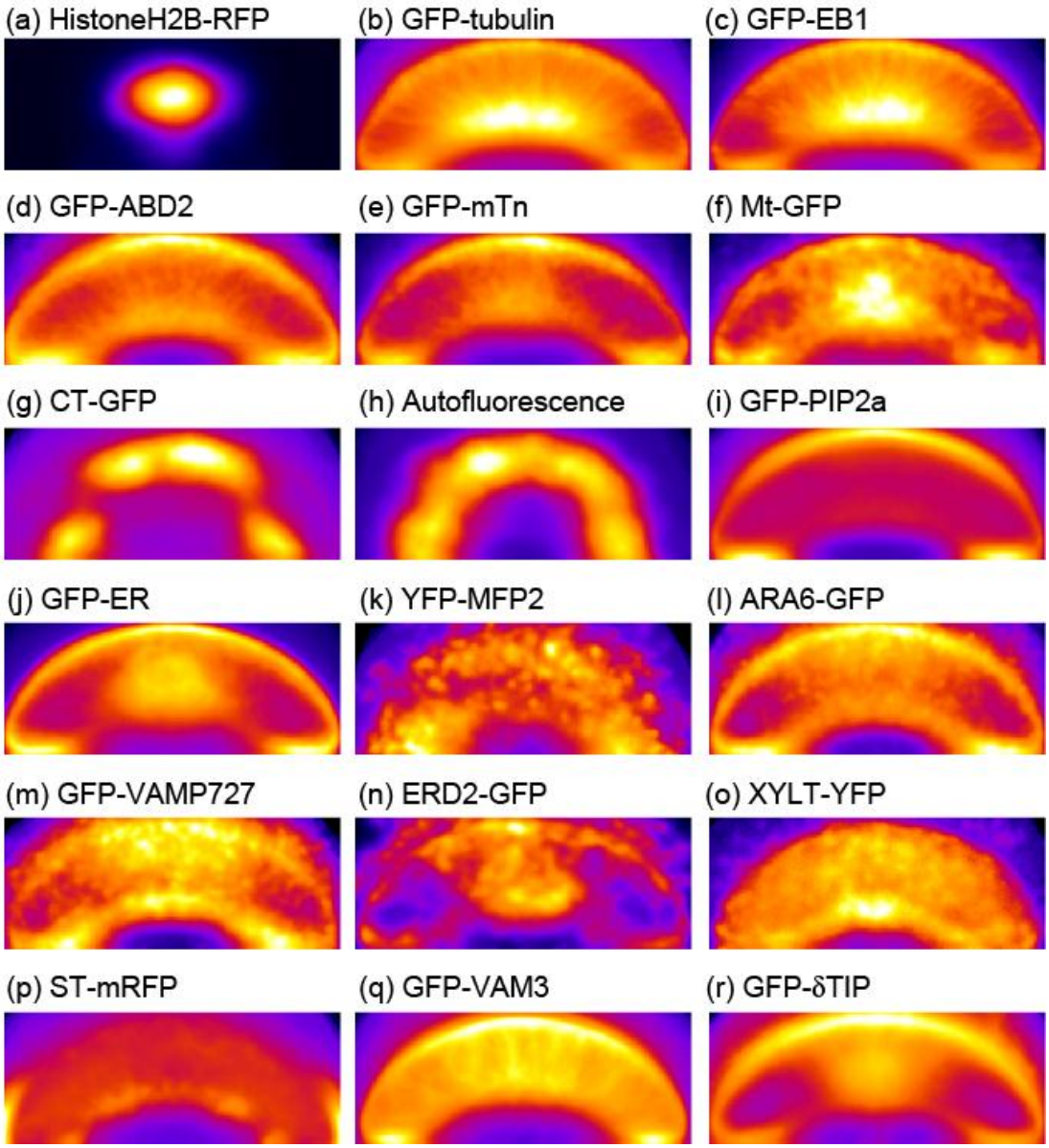

Supplementary Figure 3. Group-averaged image for each probe. (a) Cell nuclei labeled by HistoneH2B-RFP; (b) Microtubules labeled by GFP-tubulin; (c) Microtubule plus-end labeled by GFP-EB1; (d, e) Actin microfilaments labeled by GFP-ABD2 (d) and GFP-mTn (e); (f) Mitochondria labeled by Mt-GFP; (g, h) Chloroplasts labeled by CT-GFP (g) and autofluorescence (h); (i) Plasma membrane labeled by GFP-AtPIP2a; (j) Endoplasmic reticulum labeled by GFP-ER; (k) Peroxisomes labeled by YFP-MFP2; (l, m) Endosomes labeled by ARA6-GFP (l) and

GFP-VAMP727 (m); (n) *cis*-Golgi labeled by ERD2-GFP; (o) *medial*-Golgi labeled by XYLT-YFP; (p) *trans*-Golgi labeled by ST-mRFP; and (q, r) Vacuolar membranes labeled by GFP-VAM3 (q) and GFP-δTIP (r). These images were obtained from 100-120 guard cells. To facilitate visualization, images are presented in pseudo color. All of the image sizes were normalized into a mean size of 304 × 119 pixels (19.5 × 7.6 μm). Note that none of these images were folded but rather showed a symmetrical distribution in all the probes used.

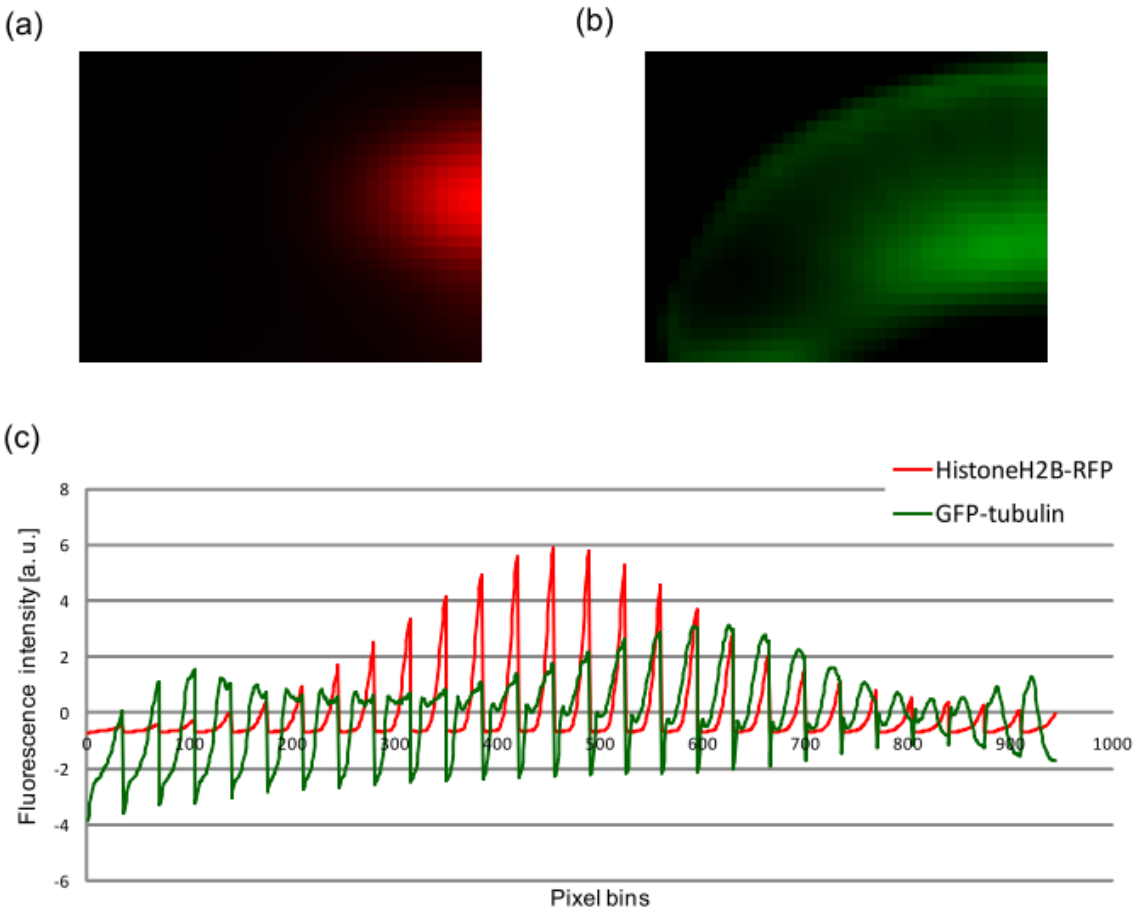

Supplementary Figure 4. Raster-scanned intensity profile. (a, b) The half-separated probability maps of cell nuclei labeled by HistoneH2B-RFP (a) and microtubules labeled by GFP-tubulin (b). (c) Raster-scanned intensity profiles of HistoneH2B-RFP (red) and GFP-tubulin (green). We normalized the half-separated image sizes to 35 × 27 pixels, and then measured and used the intensities in the 945 pixel bins as metric patterns for image clustering.

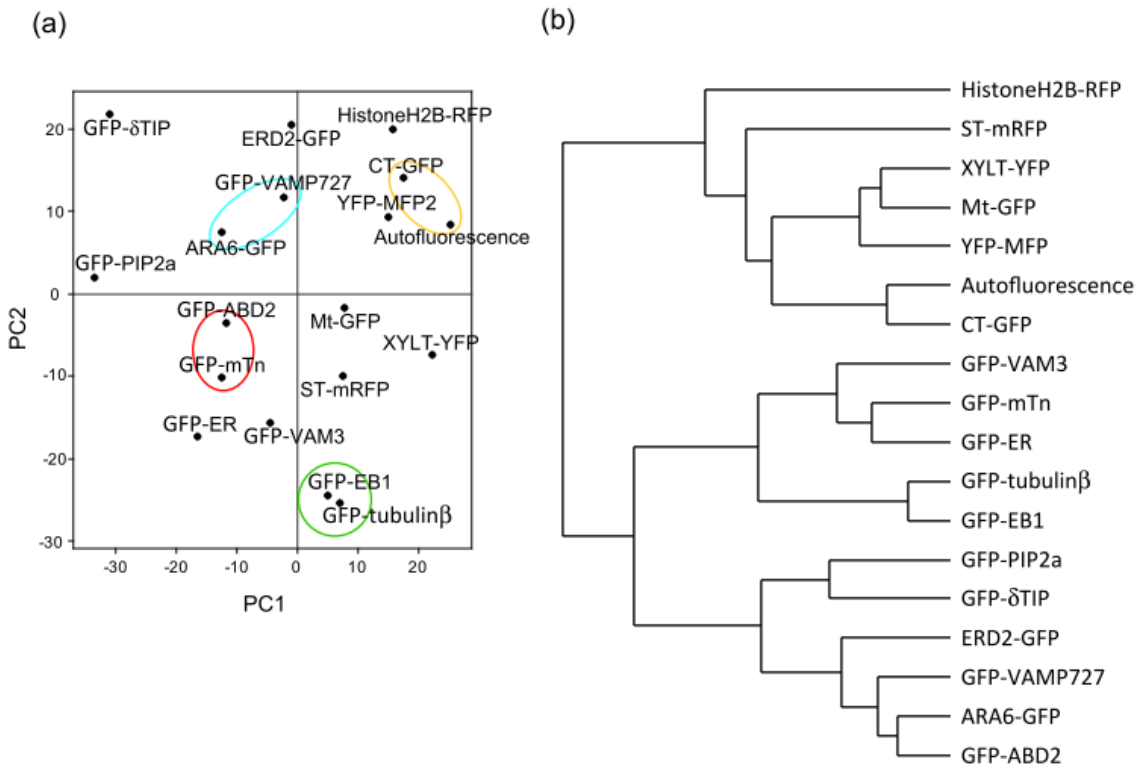

Supplementary Figure 5. Clustering of probability maps. (a) Principle component analysis (PCA) based on the sample correlation matrix. The colored circles show similarly-targeted fluorescent markers. (b) Hierarchical clustering. The dendrogram was produced using Euclidean distance and Ward's algorithm. The clustering was based on the raster-scanned intensity profiles shown in **Supplementary Figure 4**.

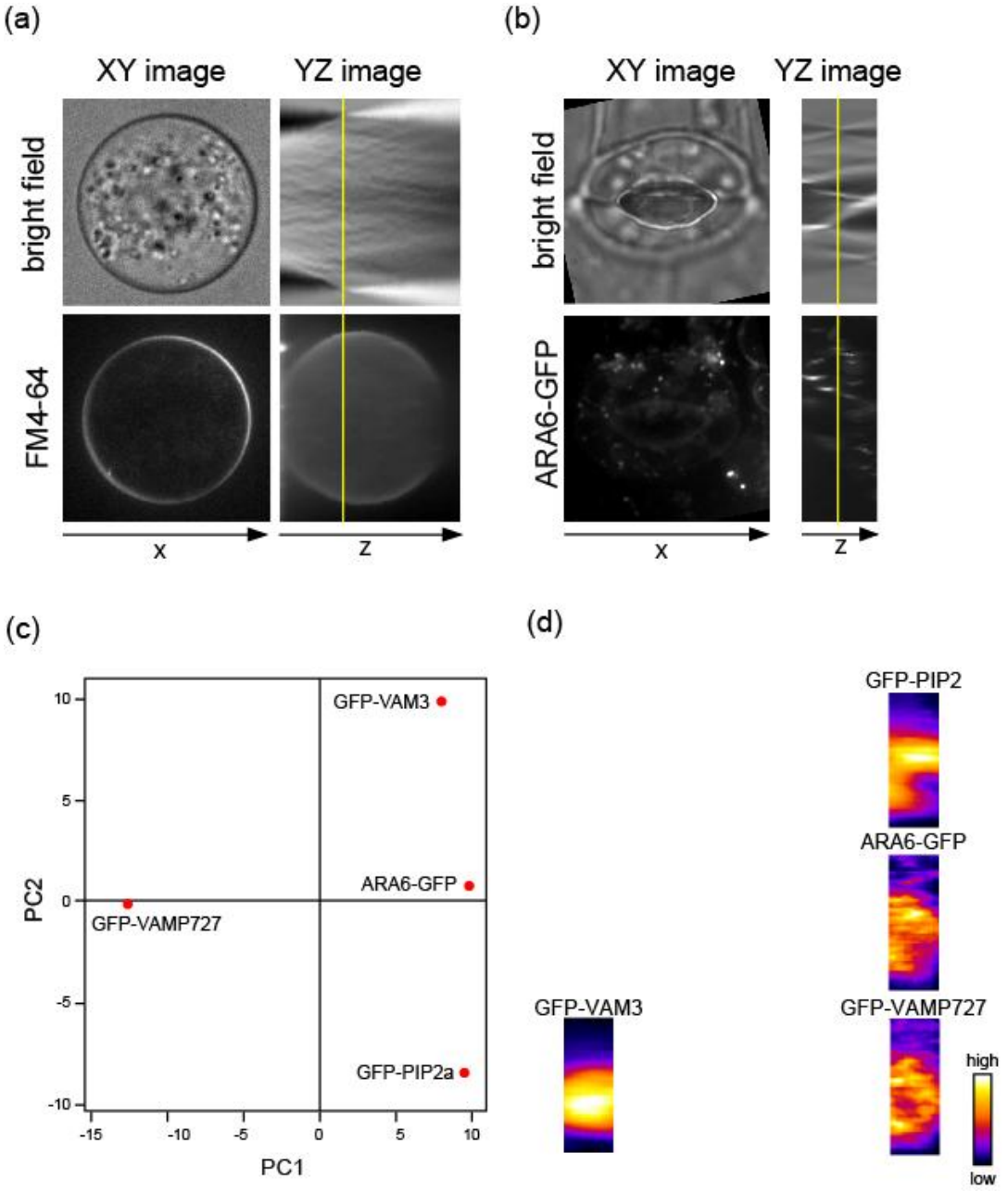

Supplementary Figure 6. Analysis of the YZ sectional images. (a, b) Registration of Z-axis using serial sections of bright field images. A spherical tobacco BY-2 miniprotoplast stained with FM4-64 for 2 min was shown as an example (a). The fluorescence of FM4-64 indicates the plasma membrane. We found low and high intensity regions along the cell periphery in the YZ section of bright field images. The cross-point, which is indicated by the yellow line, was at a position in which the plasma

membrane is vertical to the objective lens, suggesting that the cross-point is useful for Z-axis registration. Similar to miniprotoplasts, we could detect the cross-point along the guard cell membrane of guard cells expressing ARA6-GFP (b). We manually determined the cross-point using the YZ sections of bright filed images as shown by the yellow lines, and then aligned the Z-axis position to produce a probability map of the YZ sections shown in **Figure 4**. (c, d) Clustering of the probability maps of YZ sections of GFP-PIP2a, ARA6-GFP, GFP-VAMP727 and GFP-VAM3. (c) Principle component analysis (PCA) based on the sample correlation matrix. (d) Hierarchical clustering. The dendrogram was produced using Euclidean distance and Ward algorithm. The clustering was based on the raster-scanned intensity profiles shown in **Supplementary Figure 4**.

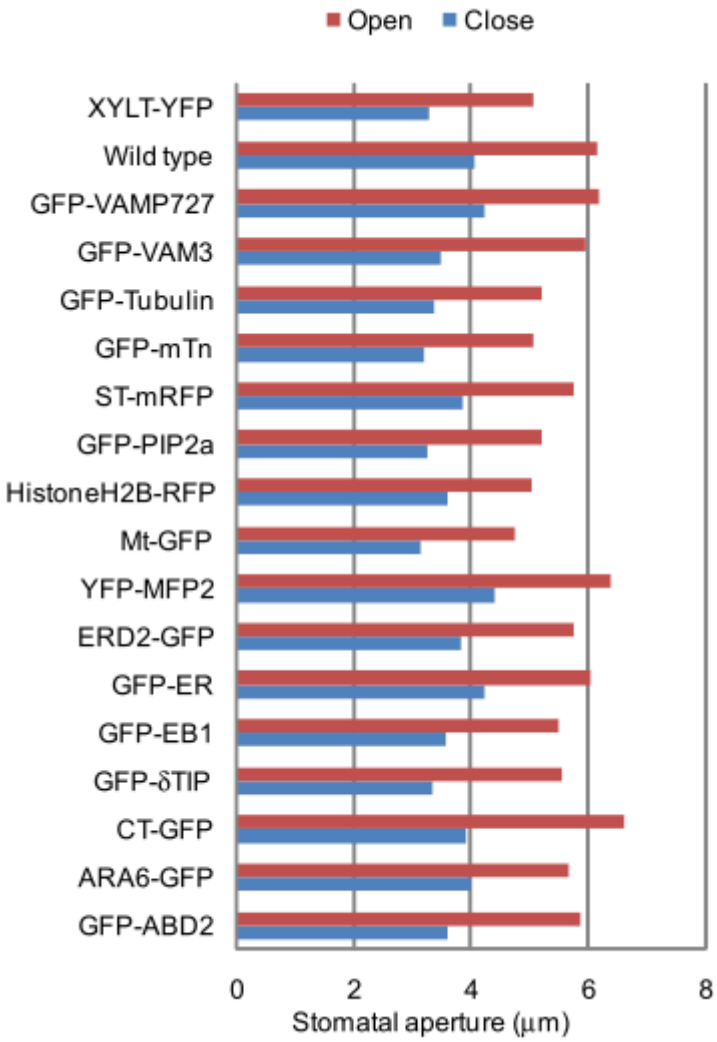

Supplementary Figure 7. Stomatal movement in wild type and transgenic Arabidopsis used in this study. The red and blue bars represent the average stomatal apertures of the top (red, Open) and bottom (blue, Close) 30 % of stomatal apertures. Note that all plant lines showed stomatal movement.

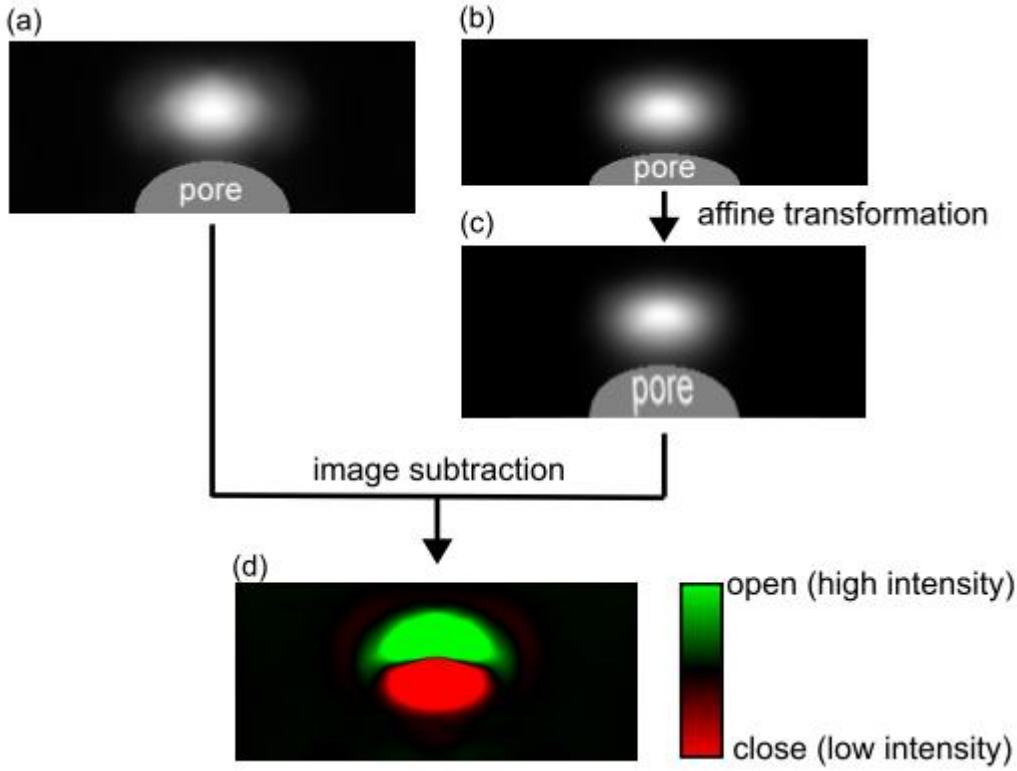

Supplementary Figure 8. Image processing for subtraction of opened and closed stomatal images. (a) The probability map of HistoneH2B in the open stomata. The pore region was segmented as a half-ellipse based on the mean stomatal apertures. This map was obtained from group-averaged images from 30 guard cells. The image size was normalized to a mean size of 303 × 128 pixels (19.4 × 8.2 μm). (b) The probability map of closed stomata. The pore region was segmented as a half-ellipse based on the mean stomatal apertures. This map was obtained from group-averaged images from 30 guard cells. The image size was normalized into a mean size of 308 × 109 pixels (19.7 × 7.0 μm). (c) Registered probability map of the closed stomata. The closed probability maps were registered into the open stomata image size of 303 × 128 pixels (19.4 × 8.2 μm) with the same pore region of open stomata using affine transformation. (d) The subtractive image from an open stomatal image (a) and the registered closed stomatal image (c). The subtractive image is shown in pseudocolor.

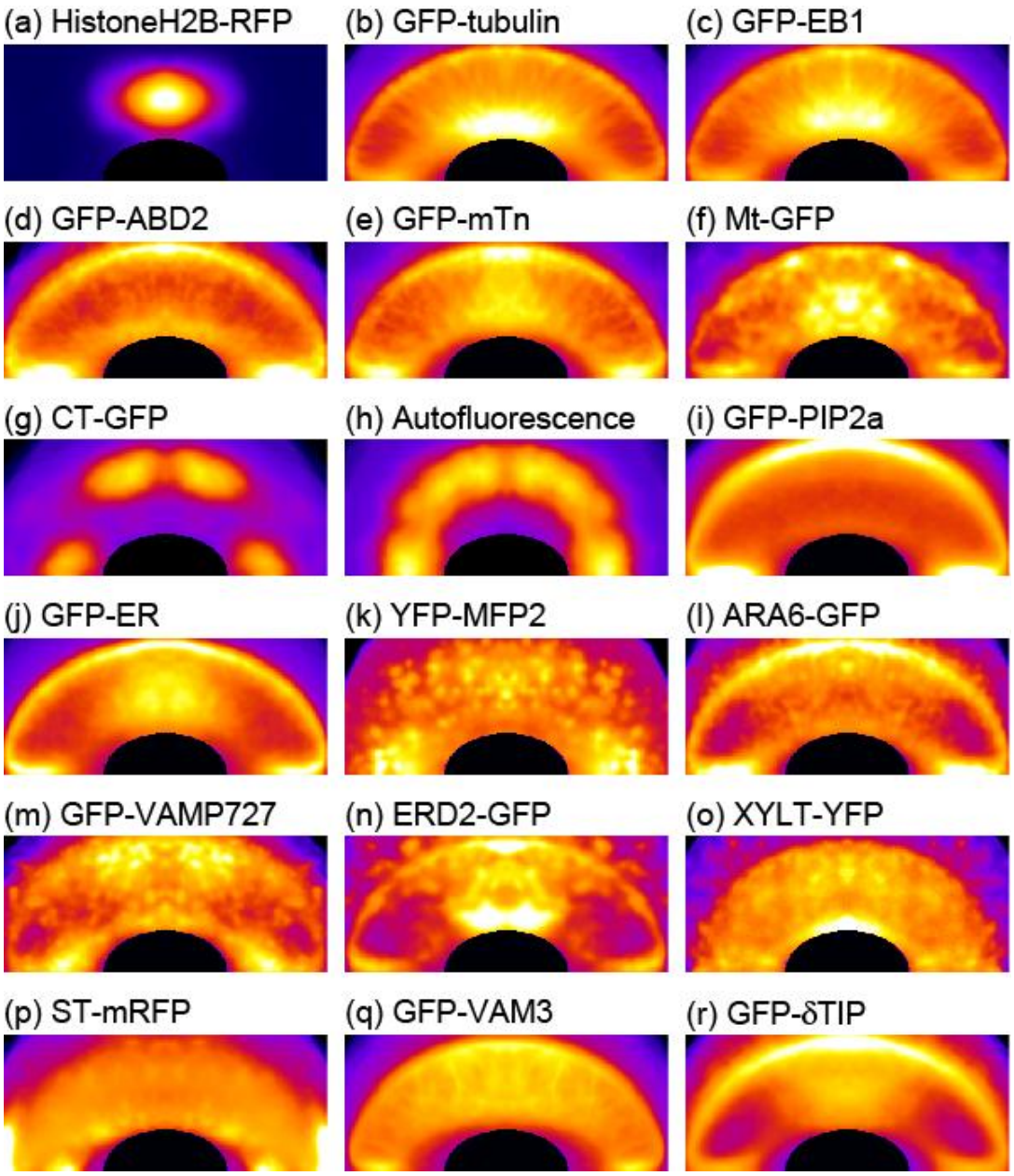

Supplementary Figure 9. Probability map of open stomatal guard cell for each probe. (a) Cell nuclei labeled by HistoneH2B-RFP; (b) Microtubules labeled by GFP-tubulin; (c) Microtubule plus-end labeled by GFP-EB1; (d, e) Actin microfilaments labeled by GFP-ABD2 (d) and GFP-mTn (e); (f) Mitochondria labeled by Mt-GFP; (g, h) Chloroplasts labeled by CT-GFP (g) and autofluorescence (h); (i) Plasma membrane labeled by GFP-AtPIP2a; (j) Endoplasmic reticulum labeled by GFP-ER; (k)

Peroxisomes labeled by YFP-MFP2; (l, m) Endosomes labeled by ARA6-GFP (l) and GFP-VAMP727 (m); (n) *cis*-Golgi labeled by ERD2-GFP; (o) *medial*-Golgi labeled by XYLT-YFP; (p) *trans*-Golgi labeled by ST-mRFP; and (q, r) Vacuolar membranes labeled by GFP-VAM3 (q) and GFP-δTIP (r). These images were obtained from 30-36 guard cells. To facilitate visualization, images are presented in pseudo color. All of the image sizes were normalized into a mean size of 303 × 128 pixels (19.4 × 8.2 μm).

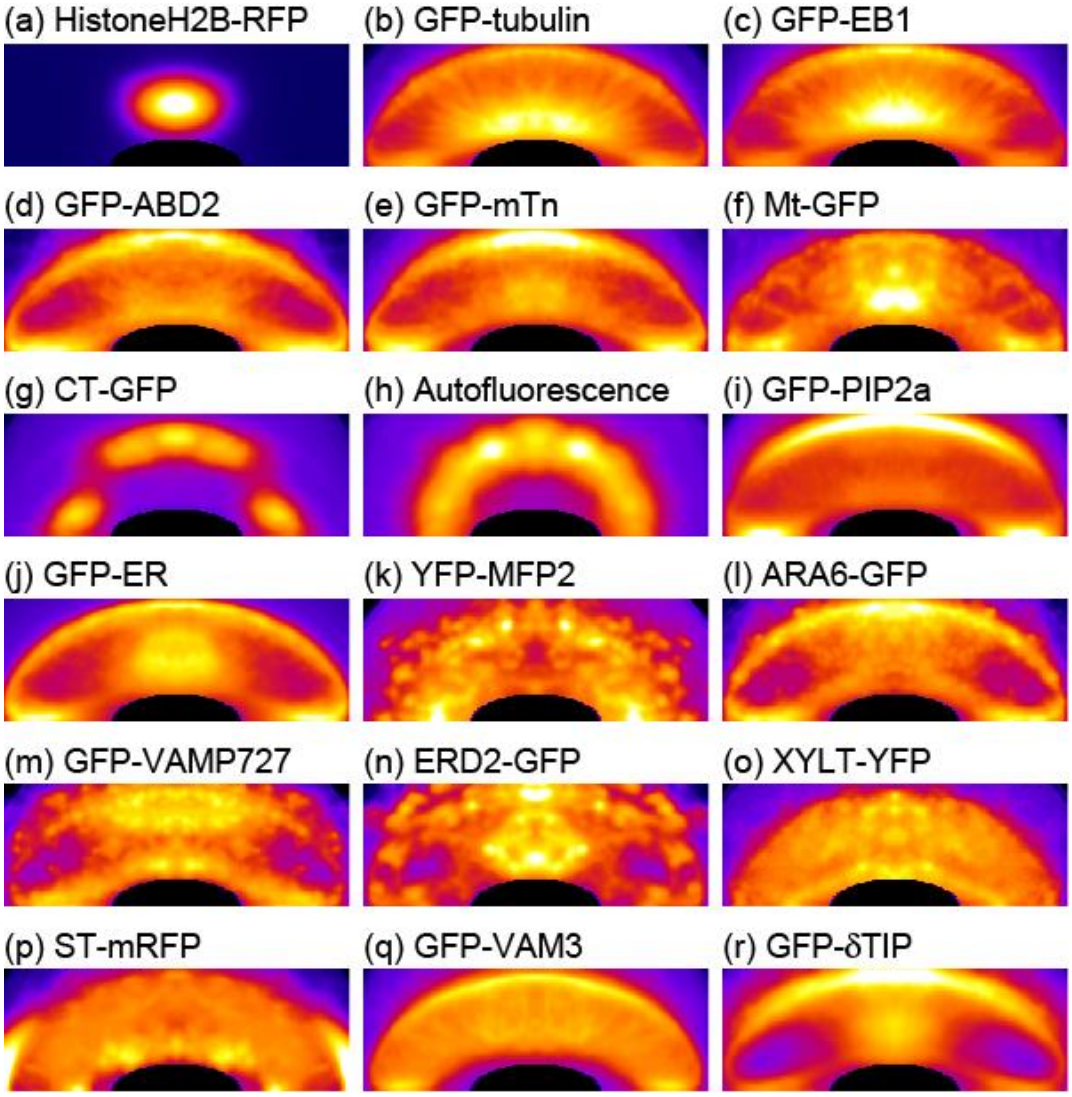

Supplementary Figure 10. Probability map of closed stomatal guard cell for each probe. (a) Cell nuclei labeled by HistoneH2B-RFP; (b) Microtubules labeled by GFP-tubulin; (c) Microtubule plus-end labeled by GFP-EB1; (d, e) Actin microfilaments labeled by GFP-ABD2 (d) and GFP-mTn (e); (f) Mitochondria labeled by Mt-GFP; (g, h) Chloroplasts labeled by CT-GFP (g) and autofluorescence (h); (i) Plasma membrane labeled by GFP-AtPIP2a; (j) Endoplasmic reticulum labeled by GFP-ER; (k) Peroxisomes labeled by YFP-MFP2; (l, m) Endosomes labeled by ARA6-GFP (l) and GFP-VAMP727 (m); (n) *cis*-Golgi labeled by ERD2-GFP; (o) *medial*-Golgi labeled by XYLT-YFP; (p) *trans*-Golgi labeled by ST-mRFP; and (q, r)

Vacuolar membranes labeled by GFP-VAM3 (q) and GFP-δTIP (r). These images were obtained from 30-36 guard cells. To facilitate visualization, images are presented in pseudo color. All of the image sizes were normalized into a mean size of 308 × 109 pixels (19.7 × 7.0 μm).

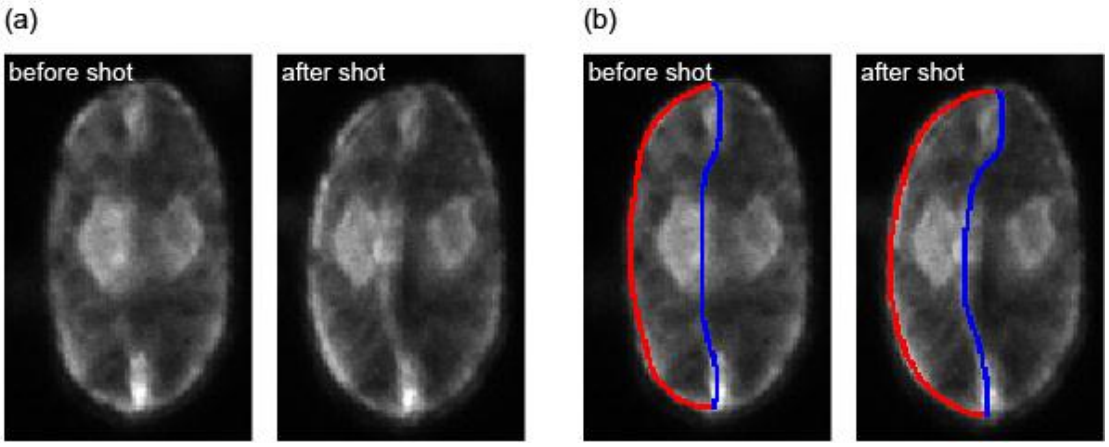

Supplementary Figure 11. Measurements of GFP-ER fluorescence intensities. (a) An example of time-lapse images. (b) The line segmentation in (a) for measurement of mean fluorescence intensity. We manually set the 2 pixel-width lines along the dorsal side (red) and ventral side including connecting region (blue) and measured the mean intensity on the lines.